International Journal of Biological Macromolecules 134 (2019) 422–434

Contents lists available at ScienceDirect

International Journal of Biological Macromolecules

journal homepage: http://www.elsevier.com/locate/ijbiomac

DNA/RNA recognition controlled by the glycine linker and the guanidine moiety of phenanthridine peptides

Josipa Matić [a], Filip Šupljika [d], Tana Tandarić [a], Marko Dukši [b], Patryciusz Piotrowski [c], Robert Vianello [a], Anamaria Brozovic [e], Ivo Piantanida [a], Carsten Schmuck [c], Marijana Radić Stojković [a,*]

[a] Division of Organic Chemistry and Biochemistry, Ruđer Bošković Institute, P. O. Box 180, 10002 Zagreb, Croatia
[b] Fidelta d.o.o., Prilaz Baruna Filipovića 29, 10000 Zagreb, Croatia
[c] Institute for Organic Chemistry, University of Duisburg-Essen, Universitätsstrasse 7, 45141 Essen, Germany
[d] Faculty of Food Technology and Biotechnology, University of Zagreb, Pierrotijeva 6, 10000 Zagreb, Croatia
[e] Division of Molecular Biology, Ruđer Bošković Institute, P. O. Box 180, 10002 Zagreb, Croatia

ARTICLE INFO

Article history:
Received 13 March 2019
Received in revised form 9 May 2019
Accepted 9 May 2019
Available online 10 May 2019

Keywords:
DNA/RNA recognition
Pyrrole guanidine peptide
DNA/RNA chiral probe

ABSTRACT

The binding of four phenanthridine-guanidine peptides to DNA/RNA was evaluated via spectrophotometric/microcalorimetric methods and computations. The minor structural modifications-the type of the guanidine group (pyrrole guanidine (GCP) and arginine) and the linker length (presence or absence of glycine)-greatly affected the conformation of compounds and consequently the binding to double- (ds-) and single-stranded (ss-) polynucleotides. GCP peptide with shorter linker was able to distinguish between RNA (A-helix) and DNA (B-helix) by different circular dichroism response at 295 nm and thus can be used as a chiral probe. Opposed to the dominant stretched conformation of GCP peptide with shorter linker, the more flexible and longer linker of its analogue enabled the molecule to adopt the intramolecularly stacked form which resulted in weaker yet selective binding to DNA. Beside efficient organization of ss-polynucleotide structures, GCP peptide with shorter linker bound stronger to ss-DNA/RNA compared to arginine peptides which emphasize the importance of GCP unit.

1. Introduction

A vast amount of biological processes, like DNA replication, transcription, translation, enzymatic reactions and many others, rely on some type of molecular recognition [1]. Noncovalent interactions that play the crucial role in these processes can be elucidated by the application of small molecules with the selective spectroscopic response observable upon binding to various DNA and RNA sequences. Besides DNA and RNA double-stranded, hybrid and multistranded structures, single-stranded nucleic acids can also be potential targets for small molecules [2]. For instance, long poly-G sequences can form a four-stranded structure - G-quadruplex or can present targets for proteins such as multisubunit human protein in human fibroblasts [3,4]. Poly (A) has a relevant significance in cell biology due to its importance in mRNA stability and translation initiation while targeting of dT-based sequences can be exploited in tRNA purification as markers for oligo (dT)-cellulose [5,6]. Such molecular probes are important for many technologies used in the molecular biology and medicine [7].

By combining interesting features of their components, peptide-based probes with heteroaromatic units occupy a prominent place in the development of DNA and RNA molecular probes [8]. While heteroaromatic unit serves as a spectroscopic reporter group and often enhances the affinity of a small molecule-probe toward polynucleotides, peptide part promotes interactions via hydrogen bonding and also enables the relatively simple build-up through the peptide coupling procedures.

Due to a strong fluorescence change upon binding to polynucleotides, phenanthridine derivatives are well known fluorescent probes [9]. Although they are mainly recognized as intercalators, it is known that small modifications can turn them into minor groove binders [10]. It has been established that substituents at the C3 and C8 position of phenanthridine influence the spectroscopic response in the UV/Vis and fluorescence, [11,12] and also determine the mutagenicity of some phenanthridine derivatives, like ethidium-bromide [13,14]. For instance, a bis-phenanthridine triamine acted as a fluorimetric probe for poly G at pH 5 while phenanthridinium-triazolyluracil peptide conjugate selectively recognized poly U [15,16]. Beside many other phenanthridine derivatives, [17–19] a series of water-soluble phenanthridine peptides has also been prepared and their DNA/RNA binding affinity was evaluated in our group [16,20,21].

* Corresponding author.
E-mail address: mradic@irb.hr (M.R. Stojković).

https://doi.org/10.1016/j.ijbiomac.2019.05.063
0141-8130/

While there are many receptors reported in literature with incorporated ammonium groups as analogy to lysine, only few have been designed which utilize the corresponding arginine analogues - guanidine moieties - for phosphate recognition [22]. Owing to its positive charge over a broad range of pH values, the guanidine group can participate in electrostatic interactions and act as an efficient hydrogen bond donor [23]. Intriguingly, some guanidinocarbonyl-pyrrole (GCP) derivatives have shown a remarkably selective recognition of substrates in water [24–26]. It was shown that incorporation of this arginine analogue in peptides can transform them into efficient vectors for gene delivery while a combination of GCP motif with aromatic units enabled selective recognition of DNA or RNA sequences [27–30]. Recently, it was shown for the first time that GCP unit can recognize single-stranded RNA sequences by two nucleobase–GCP isosteric conjugates [31].

Inspired by the DNA/RNA recognition potential of the GCP motifs and taking advantage of our experience in phenanthridine derivatives [9], we designed phenanthridine peptides with GCP units (**1**, **2**) and investigated their interactions with DNA and RNA targets. We also prepared phenanthridine derivatives with arginine (**3**, **4**) to see the difference between guanidine interacting units (GCP vs Arg). The compounds additionally differed in the linker length, more precisely in the presence (**2**, **4**) or absence (**1**, **3**) of one glycine residue. The glycine residue may provide the conformational flexibility to peptides which in turn can influence interactions with polynucleotides [32,33].

It is known from literature that the heterocyclic nitrogen of phenanthridine is protonated under acidic conditions ($pK_a \approx 6$) [9] suggesting that **1**–**4** are in a protonated state at pH 5.0. Further, the connection of the guanidinium group via an acetyl group to the pyrrole decreased the pK_a value of the free guanidine (**3**, **4**) from 13.5 to approximately 6–7 for GCP unit (**1**, **2**) [34]. Thus, it can be assumed that **1** and **2** possess two positive charges at pH 5.0 while at pH 7.0 only GCP unit may be partially protonated. On the other hand, arginine derivatives, **3** and **4** possess two positive charges at pH 7.0 and three positive charges at pH 5.0.

Thus, the aim of this work was to investigate the recognition of nucleic acids by phenanthridine peptides. This recognition was evaluated in dependence of several factors: a) two minor structural modifications in peptides **1**–**4**: 1) differently protonated guanidine moieties in arginine- and guanidinocarbonylpyrrole-based phenanthridine peptides and 2) the peptide linker differing in presence or absence of glycine (Scheme 1) b) pH of the solution c) the secondary structure of the polynucleotides and basepair composition of ds- and ss-polynucleotides. Interactions with double-stranded (*ds*-) and single-stranded (*ss*-) DNA and RNA were analysed via spectrophotometric (fluorimetric titrations, thermal melting experiments and CD titrations) and microcalorimetric methods, and rationalized by the computational analysis.

Previously studied phenanthridine-alanine (**Ala-Phen**, Scheme 2) [20,21] was used as a starting material for new probes (Scheme 3) which are obtained through classical peptide coupling in solution. Two of here studied phenanthridine-peptide derivatives with GCP unit (**1**, **2**) have already shown a micromolar affinity to the dipeptidyl peptidase III (DPP III) and an inhibition of hydrolysis of Arg-Arg-2-naphthylamide, the standard synthetic substrate of DPP III [35].

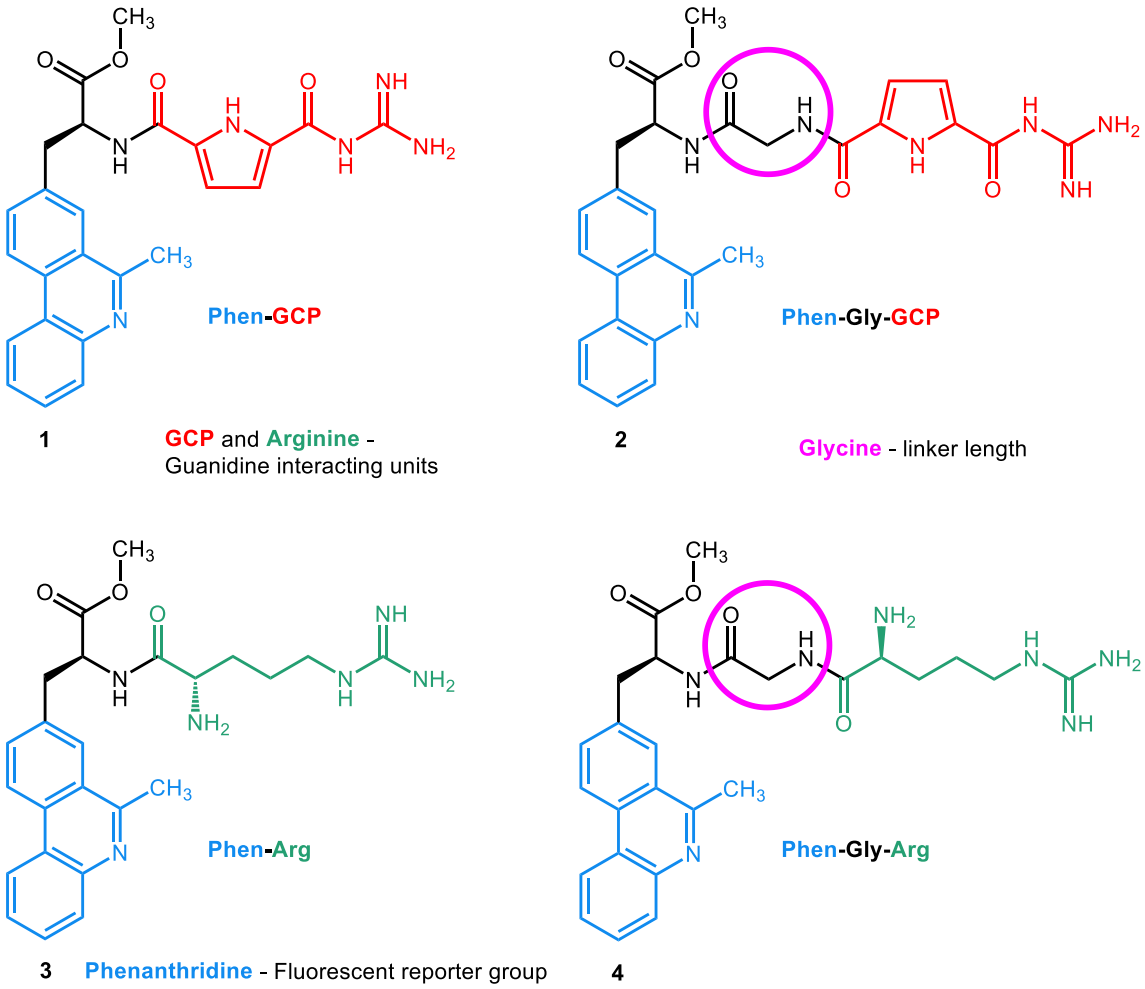

Scheme 1. Schematic presentation of studied compounds **1**–**4**.

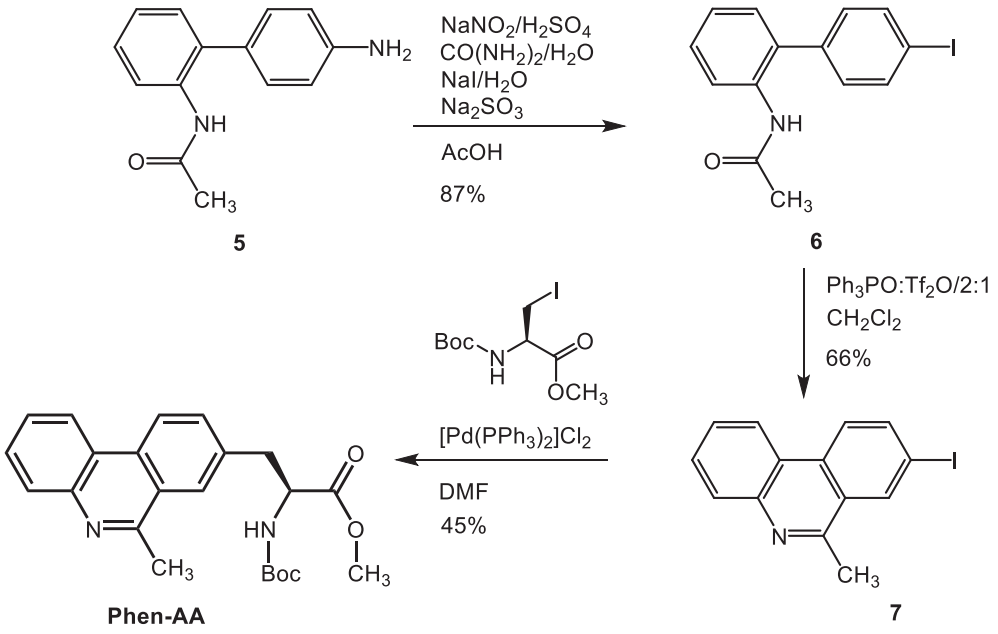

Scheme 2. Synthesis of **Phen-AA**, starting from 4′-amino-2-acetamidobiphenyl **5**.

2. Results

2.1. Synthesis

8-Iodo-6-methylphenanthridine **7** was prepared in five steps, starting from commercially available 2-aminobiphenyl. Two synthetic steps leading to 4′-amino-2-acetamidobiphenyl **5** have been described previously [36,37]. It was used as a starting compound for a Sandmeyer-type reaction, which provided 4′-iodo-2-acetamidobiphenyl **6**. Intramolecular Friedel–Crafts cyclization of iodo-biphenyl derivative **6** into 8-iodo-6-methylphenanthridine **7** was achieved using Hendrickson reagent [38]. Iodoserine was prepared according to the known procedure [39].

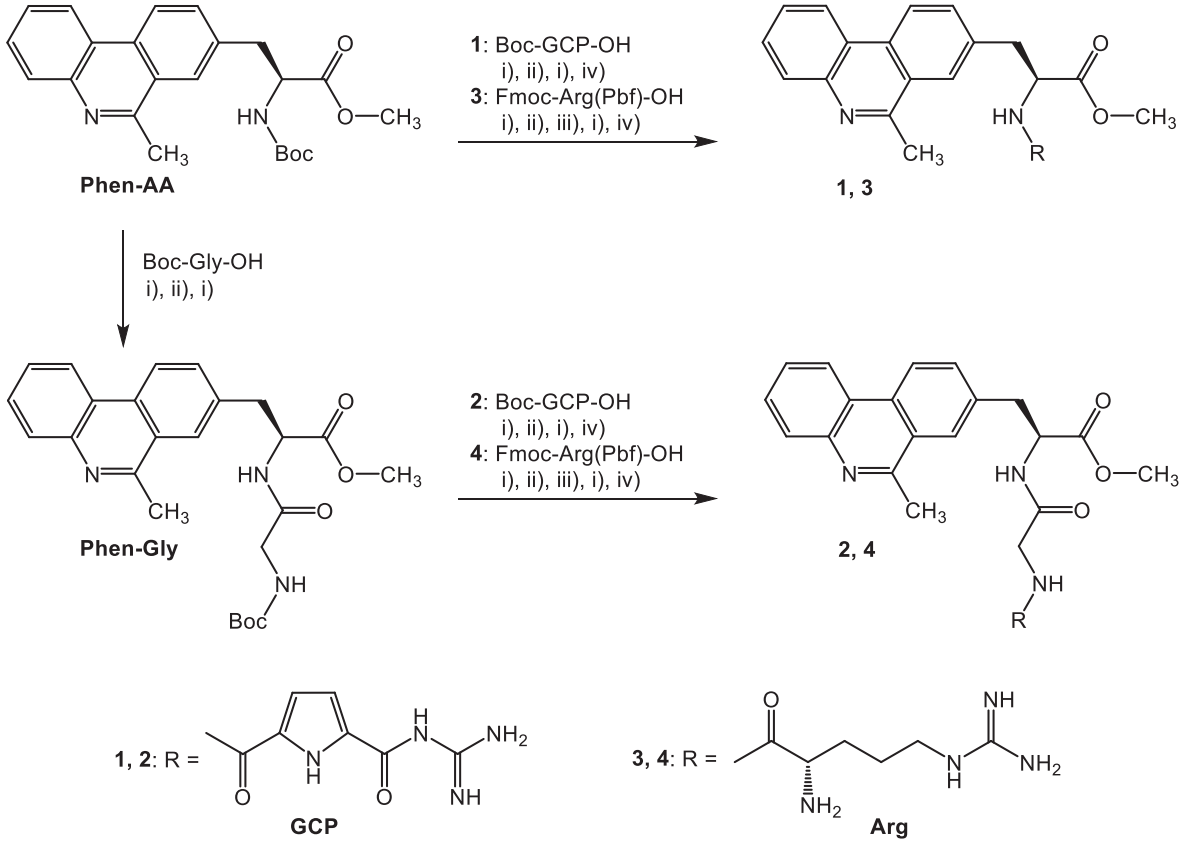

Scheme 3. Preparation of **1**, **2**, **3** and **4** starting from **Phen-AA** and **Phen-Gly**, by reaction procedure: i) TFA:H_2O/9:1, CH_2Cl_2, r.t.; ii) HBTU, HOBT, Et_3N, CH_3CN, r.t.; iii) 1% piperidine in CH_2Cl_2, r.t. iv) 5% HCl_{aq}, MeOH.

Phen-AA was synthesized by palladium-catalyzed Negishi cross-coupling of 8-iodo-6-methylphenanthridine **7** and iodoserine (Scheme 2) [40].

Novel phenanthridine derivatives (**1**–**4**) were prepared by coupling of previously described **Phen-AA** and **Phen-Gly** with selected HBTU-activated carboxylic acids [20]. Solution-phase peptide synthesis yielded **1**, **2**, **3** and **4** in very good to excellent yields (58–95%). Compounds **1** and **2** were prepared and transformed into hydrochloride salts as reported earlier [35]. Compounds **3** and **4** were prepared following corresponding synthetic procedures with commercially available Fmoc-Arg(Pbf)-OH, as presented on the Scheme 3. After removal of –Fmoc and –Pbf protecting groups, compounds **3** and **4** were converted to water-soluble hydrochloride salts likewise.

2.2. Spectroscopy

Compounds **1**–**4** were soluble in aqueous buffer systems up to $c \approx 2.0 \times 10^{-3}$ mol dm^{-3} (at pH 7.0 and pH 5.0, sodium cacodylate/HCl buffer, $I = 0.05$ mol dm^{-3}). Buffered aqueous solutions of studied compounds were stable for 2–4 weeks. The absorbencies of **1**–**4** (Supplementary, Figs. S1 and S2) were proportional to their concentrations up to $c = 1–3 \times 10^{-5}$ mol dm^{-3}, changes in the UV/Vis spectra of majority of studied compounds on the temperature increase up to 95 °C were negligible and the reproducibility of UV/Vis spectra upon cooling back to 25 °C was excellent. The only exception was compound **2** where the temperature increase resulted in the increase of the UV/Vis spectra (~15% at 300 nm at pH 7.0), suggesting the presence of some sort of molecular stacking. Absorption maxima of **1** and **2** and the corresponding reference compounds **Phen-AA**, **Phen-Gly** [20], **GCP** [41,42] (Table 1, Scheme 3) were very similar both in neutral and weakly acidic conditions (pH 7.0 and pH 5.0). However, a comparison of the UV/Vis spectra of **2** (at both pH) with the corresponding references **Phen-AA**, **Phen-Gly** and **GCP** (Table 1, Supplementary, Fig. S5) revealed a hypochromic effect, which, in line with above noted temperature dependence, strongly supported an intramolecular stacking interaction between phenanthridine and pyrrole chromophores.

Also, the molar absorptivity (Table 1) of **1** at pH 7.0 was smaller than the sum of molar absorptivities of corresponding references, **Phen-AA** and **GCP** suggesting an influence of intramolecular interactions. However, due to shorter and less flexible linker of **1** we assumed that the hypochromic effect of **1** at pH 7.0 was probably not the result of the intramolecular stacking between two chromophores like in case of **2**. This assumption was later confirmed by NMR and computations.

At pH 5.0 the molar absorptivities of **1** and its reference compound, **Phen-AA** were almost the same pointing to an absence of intramolecular interactions.

The emission intensities (Supplementary, Figs. S3 and S4) of buffered aqueous solutions (sodium cacodylate buffer, $I = 0.05$ mol dm^{-3}, pH 7.0 and pH 5.0) of studied compounds were proportional to their concentrations up to $c = 6 \times 10^{-6}$ mol dm^{-3}. The excitation spectra agreed well with the corresponding absorption spectra in the region where emission and excitation spectrum do not overlap. Significant shift of fluorescence maxima for $\Delta\lambda = 2$ 0–30 nm upon pH change from 7.0 to 5.0 observed for all compounds could be attributed to the protonation of the phenanthridine fluorophore.

The emission intensities of **3** and **4** were similar to those of reference compounds (**Phen-AA**, **Phen-Gly**), while GCP analogues **1** and **2** exhibited an order of magnitude weaker emission intensities (Table 1). Further, the fluorescence of **1** and **2** was stronger in neutral conditions than at pH 5.0. Also, the fluorescence of **1** was stronger compared to that of **2**, which could be attributed to the aforementioned intramolecular stacking of **2** (Table 1, Supplementary, Figs. S3 and S4), latter additionally supported by the CD, NMR spectra and computational studies.

Namely, ^{1}H NMR spectra of Boc-**2** (in CD_3CN) were compared with those of shorter analogue, Boc-protected **1** and the corresponding reference, **Phen-AA**. Upfield-shifted proton signals of phenanthridine (H10, H9 and H7) and pyrrole were observed only for **2**, which could be attributed to aromatic stacking interactions (Supplementary, Figs. S6–S9). Moreover, the NOESY spectra of Boc-protected **2** in CD_3CN revealed a correlation between pyrrole and phenanthridine H2 proton signals. In addition, cross-peaks between pyrrole and phenanthridine protons and pyrrole and a phenanthridine-CH_3 group of deprotected **2** (hydrochloride salt) detected in D_2O, also suggested the presence of stacked structures (Supplementary, Fig. S9). In contrast to **2**, NOESY spectra of Boc-protected **1** in CD_3CN as well as of deprotected **1** in D_2O did not reveal any significant correlations between phenanthridine and pyrrole suggesting an absence of stacked conformation, which is further confirmed by computational simulations (Section 2.5, see later).

CD spectra of **2** at both pH values (Fig. 1) were characterized by a negative and a positive CD band of similar intensities, located at 309 nm and 254 nm, respectively. Those wavelength values correspond to the absorption maxima of phenanthridine and pyrrole chromophores in **2**. Such bisignate CD signal, that can point to the formation of intramolecular or intermolecular dimers [45–47], agreed well with the hypochromic effect noticed in UV/Vis spectra of **2**. In contrast to **2**, in CD spectrum of **1** only negative CD bands were detected, at 240 nm and

Table 1
Electronic absorption maxima and corresponding molar extinction coefficients in aqueous medium,[a,b] fluorescence emission maxima and corresponding relative quantum yields.[c]

	UV/Vis		Fluorescence emission Q^c		
	λ_{max} (nm)/$\varepsilon \times 10^3$ (dm^3 mol^{-1} cm^{-1})				
	pH 5.0	pH 7.0	λ_{max} (nm)	pH 5.0	pH 7.0
1	252/46.2 298/32.2	251/30.3 300/21.4	401[a]/372[b]	0.01	0.02
2	252/38.6 300/19.6	252/39.5 300/17.7	400[a]/372[b]	<0.01	0.01
Phen-AA	251/49.5 300/4.8	250/50.6 300/4.5	402[a]/370[b]	0.16	0.25
Phen-Gly	251/51.9 300/5.1	250/53.7 300/4.8	403[a]/370[b]	0.21	0.33
3	251/49.5	250/50.6	388[a]/372[b]	0.25	0.34
4	251/51.9	250/53.7	398[a]/372[b]	0.14	0.24
GCP	250/4.0 297/27.3	250/6.1 297/28.4	–	–	–

[a] Buffer pH 5.0 (sodium cacodylate buffer, $I = 0.05$ mol dm^{-3}).
[b] Buffer pH 7.0 (sodium cacodylate buffer, $I = 0.05$ mol dm^{-3}).
[c] Relative quantum yield (Q) was determined with respect to L-*N*-acetyltryptophanamide (NATA) standard ($Q = 0.14$) [43,44].

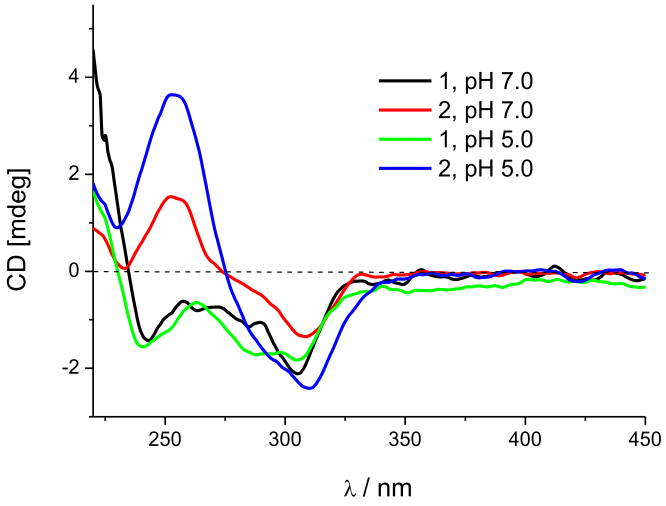

Fig. 1. CD spectra of **1** and **2** in Na-cacodylate buffer ($I = 0.05$ mol dm^{-3}, pH 5.0 and pH 7.0); c(**1**, **2**) $= 1.5 \times 10^{-5}$ mol dm^{-3}.

306 nm at both pH while at pH 5.0 an additional negative signal appeared at 288 nm.

Positive CD bands near 250 nm, which correspond to the absorption maxima of phenanthridine were visible in CD spectra of **3** at both studied pH (Supplementary, Figs. S10–S11). In contrast to **3**, in CD spectra of **4** which possess the longer linker, there was no noticeable positive CD band at 250 nm at pH 7.0 (Supplementary, Fig. S10). At pH 5.0, protonated form of **4** produced CD bands of noticeable intensities in the area from 235 to 290 nm but unlike **3** there was no well-defined maximum at 250 nm (Supplementary, Fig. S11).

2.3. Study of interactions of *1–4* with ds-polynucleotides in aqueous medium

2.3.1. Spectrophotometric titrations

Binding of studied compounds to polynucleotides was monitored with the fluorescence spectroscopy. For an initial examination with ds-polynucleotides, we have chosen *calf thymus* DNA (42% of GC basepairs and 58% of AT basepairs), which represents a classical B-helix, and poly A – poly U as a model for RNA, with characteristic A-helical structure of a wide and shallow minor groove and a deep and narrow major groove [48]. Different protonation states of studied compounds enabled a determination of binding affinities in both neutral (pH 7.0) and weakly acidic (pH 5.0) conditions. Mostly, higher binding affinities toward polynucleotides were observed at pH 5.0 compared to pH 7.0, which can be related to an increased number of ligands' positive charges at lower pH. Due to that reason, the binding interactions of studied compounds at pH 5.0 were further investigated with synthetic ds-polynucleotides (poly(dAdT)$_2$ and poly(dGdC)$_2$).

The addition of DNA and RNA polynucleotides (at excess of a polynucleotide, Fig. 2, Supplementary Figs. S12–S19 and S28–S43) yielded a decrease in emission intensities of all studied compounds. In general, GC-containing DNAs induced a stronger quenching of fluorescence in comparison to AT(U)-polynucleotides, whereby the most pronounced difference was observed for **2** (Table 2), being fluorimetricaly specific for GC-containing polynucleotides. Such general emission quenching proportional to GC-basepair content in polynucleotide could be correlated to the well-known redox potential of nucleobases, guanine base being the most electron-donating of all four nucleobases, and for that reason known to quench the emission stronger [49–51].

Interestingly, in GCP-based peptides, a stronger decrease in fluorescence of **1** (shorter linker) than **2** (longer linker) was noticed. In contrast to GCP-based peptides, in Arg-based peptides greater changes in fluorescence exhibited **4** (longer linker) than **3** (shorter linker).

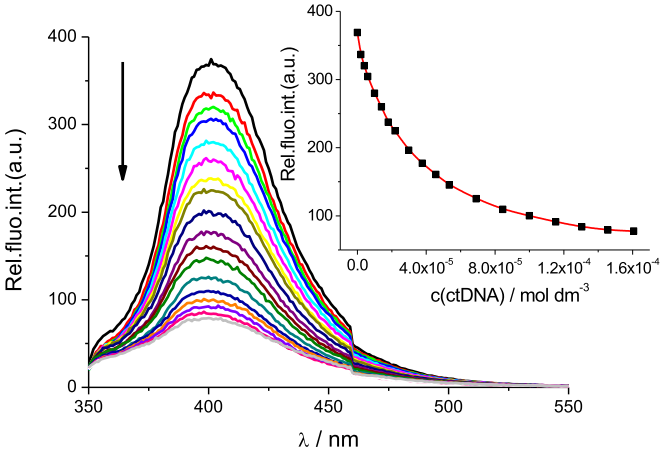

Fig. 2. Changes in fluorescence spectra of **1** ($c = 2.0 \times 10^{-6}$ mol dm^{-3}, $\lambda_{exc} = 300$ nm) upon titration with ctDNA ($c = 2.0 \times 10^{-6}$ - 1.6×10^{-4} mol dm^{-3}); Inset: Dependence of the fluorescence intensity at $\lambda_{max} = 402$ nm on c(ctDNA), at pH 5.0, sodium cacodylate buffer, $I = 0.05$ mol dm^{-3}.

Processing of fluorescence titration data collected at excess of polynucleotide over compound by means of Scatchard equation [52] gave binding constants K_a and ratios $n_{[\text{bound compound}]/[\text{polynucleotide}]}$ (Table 2). All studied compounds exerted stronger affinities toward ds-DNA than ds-RNA at pH 5.0 (Table 2). In line with a noticed trend in fluorescence changes of **1–4**, the stronger affinities toward studied polynucleotides were obtained for peptides **1** and **4** than for **2** and **3** (Table 2, Fig. 2). GCP-peptide **2** exhibited a stronger binding affinity toward ds-DNA (especially toward GC basepairs) than to ds-RNA.

2.3.2. Thermal melting experiments

A difference between T_m (melting temperature) value of free polynucleotide and their complexes with a small molecule (ΔT_m value) is an important factor in the characterisation of small molecule/ds-polynucleotide interactions (electrostatic interactions, minor groove binding, intercalation) [53].

In general, arginine-analogues **3–4** stabilised ds-polynucleotides more efficiently than GCP analogues **1–2**, likely due to the more favourable sterical and electronic properties of aliphatic guanidine (e.g. $pK_a = 13.5$ in comparison to pK_a of GCP ≈ 6). At pH 7.0 only **3** and **4** were protonated, but the stabilisation effect was observed only for **4** - poly A-poly U complex, pointing out the significance of longer linker for the binding interactions within the polynucleotide binding site (Table 3, Figs. S20 and S21).

At pH 5.0 all studied compounds were similarly protonated and showed a stabilisation of ctDNA (58% AT, 42% GC), but only Arg-based peptides **3–4** stabilised ds-RNA. Further, higher ΔT_m values were obtained for complexes of **1** and **4** with AT polynucleotides than with ctDNA (Supplementary, Figs. S44–S47). Such AT preference over mixed base pair composition noticed for **1** and **4** can be explained by dimension differences of the minor groove at AT sites and GC sites (latter being sterically hindered by the protruding amino groups of guanine) [54]. To see whether the stabilisation effect at pH 5.0 mainly originated from the electrostatic interactions, we performed thermal denaturation experiments with arginine derivatives at higher ionic strength ($I =$ 0.15 mol dm^{-3}). The results confirmed our assumption since the stabilisation of ds-DNA was much lower, while for ds-RNA completely disappeared compared to experiment at lower ionic strength ($I =$ 0.05 mol dm^{-3}).

2.3.3. Circular dichroism experiments

CD spectroscopy is a highly sensitive method that gives the insight into the conformational changes of polynucleotide properties induced by small molecule binding [56,57]. In addition, achiral small molecules can eventually acquire an induced CD spectrum (ICD) upon binding to polynucleotides, which could point to a specific, uniform orientation of small molecule with respect to helix axis and pseudo dyad axis thus giving a useful information about modes of interaction [56,58]. Nevertheless, it has to be taken into account that studied compounds are chiral and consequently possess an intrinsic CD activity. Therefore, besides performing the CD titrations with DNA and RNA, we also recorded CD spectra of free **1–4** in aqueous solution (Fig. 1 and Supplementary, Figs. S10 and S11) to more easily interpret an impact of compounds on the conformation of polynucleotide. Yet, changes in CD spectra of polynucleotides cannot be easily interpreted in the wavelength area <300 nm if ligands also absorb light in that region (Fig. 3, Supplementary, Figs. S22–S27, S48–S55 and S77–S88). Nevertheless, since **1–4** possess UV/Vis spectra also at λ > 300 nm, CD changes in this range can be attributed solely to their chromophores interacting with DNA and RNA.

At pH 7.0, arginine derivatives **3–4** did not induce significant changes in CD spectra of ctDNA and poly A–poly U (Supplementary, Figs. S24–S25), while at pH 5.0 **3** and **4** caused mainly the increase of CD spectra of DNA and RNA, with the most pronounced effect observed for GC-DNA (Supplementary, Figs. S50–S51, S54–S55). The addition of GCP derivative **1** caused negligible changes in CD spectra of DNA and RNA polynucleotides in neutral conditions. Negative ICD signals at

Table 2
Binding constants ($\log K_a$)[a] and spectroscopic properties of complexes I/I_0[b] calculated from the fluorescence titrations of **1–4** with ds-polynucleotides at pH 5.0 and pH 7.0 (buffer sodium cacodylate, $I = 0.05$ mol dm^{-3}).

Polynucleotide	1		2		3		4	
	pH 7	pH 5	pH 7	pH 5	pH 7	pH 5	pH 7	pH 5
	$\log K_a/I/I_0$[b]							
ctDNA	6.0/0.8	5.1/0.1	–[c]/–[c]	4.6/0.6	3.6/0.1	4.0/0.2	5.2/0.2	5.7/0.3
Poly(dAdT)$_2$	–[d]/–[d]	5.2/0.6	–[d]/–[d]	–[c]/–[c]	–[d]/–[d]	4.8/0.7	–[d]/–[d]	5.6/0.1
Poly(dGdC)$_2$	–[d]/–[d]	6.0/0.2	–[d]/–[d]	4.9/0.4	–[d]/–[d]	4.7/0.3	–[d]/–[d]	6.1/0.1
Poly A-poly U	6.3/0.8	4.8/0.3	–[c]/–[c]	–[c]/–[c]	3.6/0.7	4.3/0.8	4.9/0.4	5.6/0.2

[a] Accuracy of $n \pm 10$–30%, consequently $\log K_a$ values vary in the same order of magnitude; processing of titration data by means of Scatchard equation [52] gave values of ratio n[bound **1–4**]/[polynucleotide phosphate] = 0.1–0.4 for most complexes; for easier comparison all $\log K_a$ values were re-calculated for fixed $n = 0.3$; correlation coefficients were >0.99 for all calculated K_a.
[b] I_0 – starting fluorescence intensity of **1–4**; I – fluorescence intensity of **1–4**/polynucleotide complex calculated by Scatchard equation.
[c] Small fluorescence changes of **2** with polynucleotides disabled accurate calculation of binding constants.
[d] Not determined.

305 nm at pH 7.0, similar in shape but smaller in intensity compared to intrinsic CD signals of **1** were visible in CD spectra with most of the studied polynucleotides. Those changes were most evident in the case of AT- and GC-DNA (Supplementary, Fig. S26).

In contrast to neutral conditions, at pH 5.0 the addition of **1** to polynucleotide solutions resulted in positive ICD signals around 300 nm which were strongly dependent on a basepair composition (Fig. 3). Namely, the maximum of GC-induced ICD was about 292–295 nm, AT-induced at 305–308 nm and AU-induced at 312 nm. Particularly interesting is that RNA (AU)-induced CD band is at zero at 295 nm where both DNA-induced CD bands showed strong intensity. Thus, compound **1** could be used as a simple chiral probe for the differentiation of ds-RNA (A-helical structure) from ds-DNA (B-helix). Such a difference in the ICD response could be correlated to the positioning of small molecule chromophores in respect to the chiral axis of ds-helix, which again is directly related to the geometry of the small molecule binding site; a deep major groove of A-helical RNA in respect to the narrow minor groove of B-helical DNA, latter sterically restricted in the case of GC-DNA [55].

Addition of **2** at both pH conditions resulted in the appearance of a negative CD signal around 310 nm and larger (18–20 nm with ctDNA) or smaller (4–6 nm) hypsochromic shifts of CD spectra of all studied polynucleotides (Fig. 4). In a majority of titrations at both pH values, ICD signals near 310 nm obtained upon binding of **2** toward most of the polynucleotides were more negative than the intrinsic CD signals of **2**. Further, an intensity decrease of CD signal of polynucleotides at 245 nm was detected upon **2** addition which was in titration with ctDNA accompanied with the noticeable hypsochromic shift (Fig. 4). An appearance of isoelliptic points in titrations with most of polynucleotides strongly suggests one dominant interaction mode of **2** with DNA and RNA chiral axis [56,58]. Such a resemblance of CD signals of formed complexes and intrinsic CD signals of **2** suggests that **2** binds to polynucleotides in folded conformation.

2.4. Study of interactions of *1–4* with ss-polynucleotides in aqueous medium

To evaluate whether the recognition of polynucleotides by **1–4** is related to the structural features of ds-DNA and RNA or to the nucleobase-specific recognition, we also examined interactions of **1–4** with single-stranded, ss-polynucleotides. The addition of ss-polynucleotides resulted in the decrease of **1–4** fluorescence (Supplementary, S56-S76). The largest fluorescence changes were observed in titrations of **1** and **4** with poly G and poly A while highest affinities were obtained for complexes of **1** with poly G, poly U and poly dT and **4** with poly G, respectively (Table 4). In all titrations with **3** and in most of titrations with **4**, fluorescence changes were either too small to enable the accurate calculation of binding constants or linear (<20% of the complex formed), thus only the estimation of affinity was possible (Table 4, Supplementary Figs. S68–S76).

Since compound **1** showed the best binding affinities to ss-polynucleotides in fluorimetric titrations, we decided to characterize its binding thermodynamically as well. For comparison reasons, we have also done ITC titrations with its GCP analogue **2** (Table 4). All ITC titrations resulted in negative peaks indicating that the binding processes were exothermic (Table 4, Supplementary, Figs. S89–S92). The fitting model *one set of sites* was used to calculate thermodynamic

Table 3
The [a]ΔT_m values (°C) of studied ds-polynucleotides upon the addition of different ratios [b]r of **1–4** at pH 5.0 (sodium cacodylate buffer, $I = 0.05$ mol dm^{-3}) and pH 7.0 (sodium cacodylate buffer, $I = 0.05$ mol dm^{-3}).

pH	I	Compound	**1**	**2**	**3**	**4**
		[b]r=	0.5	0.5	0.3	0.3
7.0	0.05	ctDNA	0	0	−0.7	−0.9
		Poly A-poly U	0	0	0.5	3.5
5.0	0.05	ctDNA	3.4	1.4	2.1	6.5
		Poly A-poly U	0	0	1.8/0.4[c]	5.8/−1.5[c]
		Poly(dAdT)$_2$	4.5	0	–[d]	7.4
	0.15	ctDNA	–[d]		0.7	1.6
		Poly A-poly U	–[d]		0	0
		Poly(dAdT)$_2$	–[d]		–[d]	1.1

[a] Error in ΔT_m: ±0.5 °C;
[b] r = [compound]/[polynucleotide].
[c] Biphasic transitions: the first transition at $T_m = 47.3$ °C is attributed to denaturation of poly A-poly U and the second transition at $T_m = 71.1$ °C is attributed to denaturation of poly AH-poly AH since poly A at pH 5.0 is mostly protonated and forms ds-polynucleotide [55].
[d] Not determined.

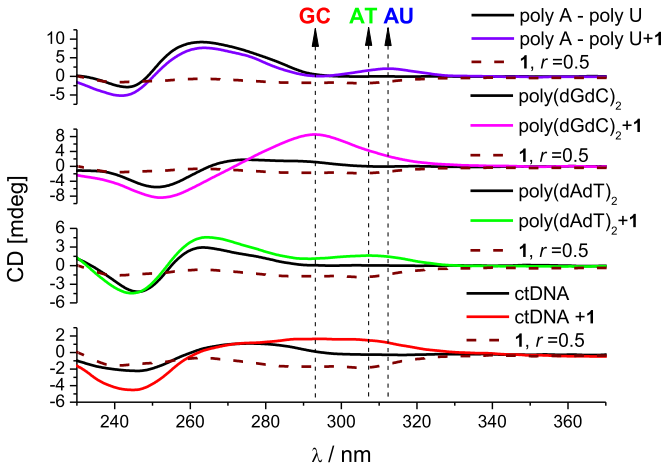

Fig. 3. CD titrations of ctDNA, poly(dAdT)$_2$, poly(dGdC)$_2$ and poly A–poly U at pH 5.0 ($c = 3.0 \times 10^{-5}$ mol dm^{-3}) with **1** at molar ratio, r [1]/[polynucleotide] = 0.5, sodium cacodylate buffer, $I = 0.05$ mol dm^{-3}.

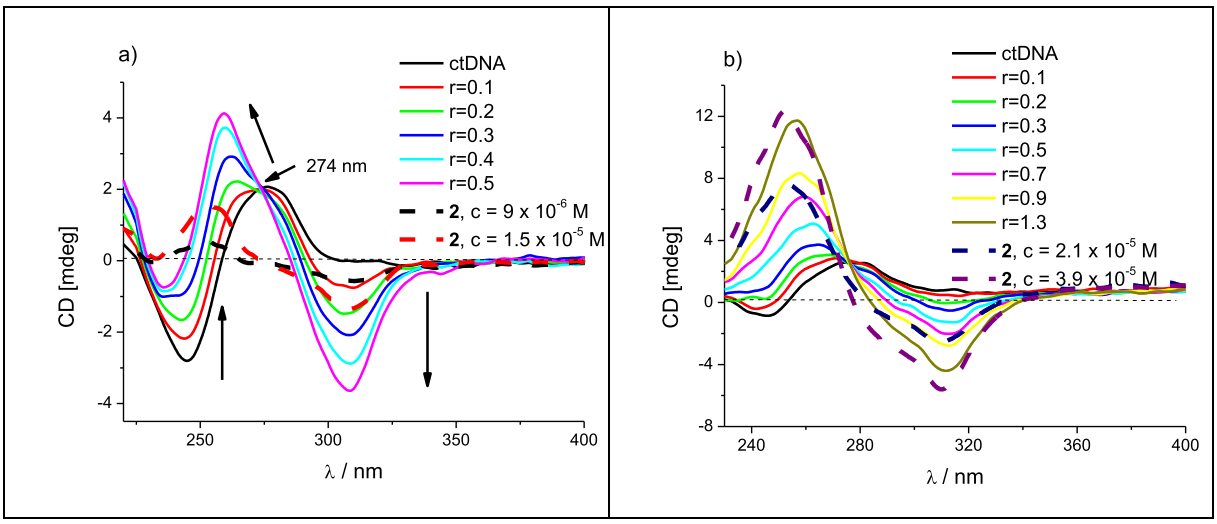

Fig. 4. CD titrations of ctDNA at a) pH 7.0 and b) pH 5.0 ($c = 3.0 \times 10^{-5}$ mol dm^{-3}) with **2** at molar ratios r = [compound]/[polynucleotide], sodium cacodylate buffer, $I = 0.05$ mol dm^{-3}.

parameters. Analysis of ITC experiments of **1** and **2** with ss-polynucleotides showed relatively high binding affinities (log K_a in Table 4) which agree well with the trend in binding affinities obtained from fluorimetric titrations. In a majority of titrations, the interaction was characterized by positive binding entropies ($T\Delta S$ term) and small negative enthalpies (see Table 4), revealing an entropically driven binding. Different thermodynamic signature was observed for the titration of **1** with poly G where the binding was favoured by larger negative enthalpy and smaller positive entropy terms.

In general, the addition of **3** and **4** to ss-polynucleotides caused negligible changes in the CD spectra (see Figs. S83–S88 in Supplementary). Exceptions were titrations of **4** with poly A, where weak negative ICD signal at λ > 300 nm appeared, (Supplementary, Fig. S84), and with poly G, (Supplementary, Fig. S88), where a strong decrease of CD bands of poly G at 260 and 290 nm were detected. In CD titration with ss-polynucleotides, compound **2** displayed similar changes as with ds-polynucleotides, namely the appearance of a negative ICD band in the 295–310 nm region and an increase of CD signal of polynucleotide with concomitant hypsochromic shift (Figs. S78, S80 and S82, Supplementary). The appearance of positive ICD signal around 312 nm was observed in most of CD titrations with **1** except in case of poly C and poly A (Fig. 5, Supplementary, Figs. S77, S79 and S81). While there was no changes with poly C, the addition of **1** to poly A resulted in very weak negative ICD spectra at λ = 300 nm (see Supplementary, Figs. S77 and S79). The ICD bands >300 nm observed for **1**, **2** could be attributed

Table 4
a) Binding constants (logK_a)[a] and spectroscopic properties of complexes I/I_0[b] calculated from the fluorescence titrations of **1**–**4** with ss-polynucleotides at pH 5.0 (buffer sodium cacodylate, $I = 0.05$ mol dm^{-3}); b) data parameters obtained during nonlinear regression for ITC titration of poly G, poly C, poly A, poly U and poly dT with compounds **1** and **2**[f] with the model one set of sites and fixed $n = 0.2$ (pH 5.0, buffer sodium cacodylate, $I = 0.05$ mol dm^{-3}).

pH 5	a) Fluorimetric titration			
	1	2	3	4
Polynucleotide	logK_a/I/I_0[b]			
Poly A	5.4/0.3	4.1/0.6	<3[d]/–[d]	4.8/0.2
Poly G	6.3/0.1	4.6/0.2	<3[d]/–[d]	6.4/0.02
Poly C	4.4/0.5	4.0/0.3	<3[d]/–[d]	<3[d]/–[d]
Poly dA	5.2/0.7	–[c]/–[c]	–[e]/–[e]	<3[d]/–[d]
Poly dT	6.5/0.7	–[c]/–[c]	–[e]/–[e]	–[e]/–[e]
Poly U	6.5/0.9	–[c]/–[c]	–[c]/–[c]	–[c]/–[c]

pH 5	b) ITC titration							
	1				**2**			
Polynucleotide	log K_a	$\Delta_r H$/kJ mol^{-1}	$T\Delta_r S$/kJ mol^{-1}	$\Delta_r G$/kJ mol^{-1}	log K_a	$\Delta_r H$/kJ mol^{-1}	$T\Delta_r S$/kJ mol^{-1}	$\Delta_r G$/kJ mol^{-1}
Poly G	5.1	−21.5	7.5	−29.0	4.5	−15.5	10.1	−25.6
Poly C[g]	5.5	−5.1	26.5	−31.6	3.8	−5.6	16.2	−21.8
Poly A	4.3	9.5	15.0	−24.5	[f]			
Poly U[g]	5.9	−8.3	25.4	−33.7	[f]			
Poly dT	5.8	2.6	35.8	−33.2	[f]			

[a] Accuracy of $n \pm 10$–30%, consequently logK_a values vary in the same order of magnitude; processing of titration data by means of Scatchard [52] equation gave values of ratio n[bound **1**–**4**]/[polynucleotide phosphate] = 0.1–0.2 for most complexes; for easier comparison all logK_a values were re-calculated for fixed $n = 0.2$, except for poly C and poly U, where we used free n; correlation coefficients were >0.99 for most of calculated K_a.
[b] I_0 – starting fluorescence intensity of **1**–**4**; I – fluorescence intensity of **1**–**4**/polynucleotide complex calculated by Scatchard equation;
[c] Small fluorescence changes of **1**–**4** with polynucleotides disabled accurate calculation of binding constants.
[d] Estimated value due to <20% of the complex formed, linear change or no change in fluorescence intensity.
[e] Not determined.
[f] Thermal changes with poly A, poly U and poly dT were too small for calculation of binding constants.
[g] Thermodynamic data were calculated using free stoichiometry ($n = 0.15$ for poly C and $n = 0.16$ for poly U) because of a more reliable fit than with fixed $n = 0.2$.

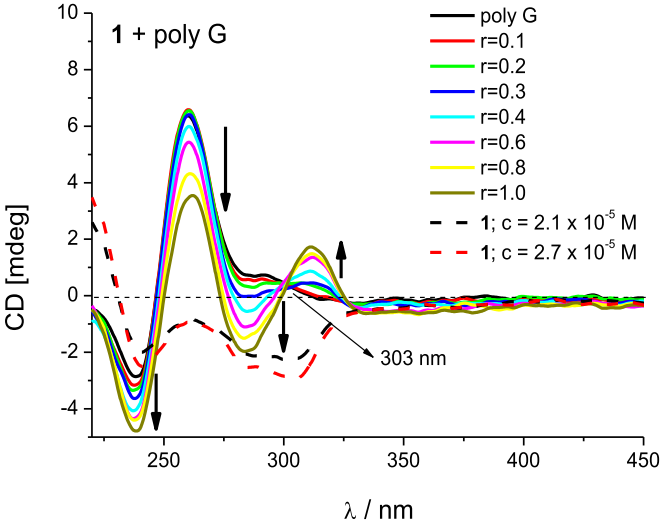

Fig. 5. CD titration of poly G ($c = 3.0 \times 10^{-5}$ mol dm^{-3}) with **1** at molar ratios $\boldsymbol{r}$ = [compound]/[polynucleotide] (pH = 5.0, buffer sodium cacodylate, $I = 0.05$ mol dm^{-3}).

to GCP unit (absorption maximum at 299 nm), since no such ICD bands were observed for **3**, **4** (lacking GCP). An efficient organization of otherwise poorly defined secondary structures of ss-polynucleotides is especially emphasized in CD titrations of **1** (Fig. 5, Supplementary Figs. S77, S79 and S81) [31].

2.5. Computational analysis of systems *1–4* in aqueous solution

In order to examine conformational features of **1**–**4**, and inspect whether their intrinsic dynamics in aqueous solution play any role in determining their ability to interact with examined polynucleotides, we performed molecular dynamics (MD) simulations of different protonation forms of **1**–**4** in explicit water and analysed structural preferences in the obtained trajectories.

In setting up our simulations, we were guided by the experimental pK_a values of the arginine side chain, isopropylamine and the phenanthridine fragment, which are 12.5, 10.6 and 5.6, respectively, [59] and assumed that these will not change much in the prepared conjugates [60]. On the other hand, previously we calculated the pK_a value for the guanidinocarbonyl-pyrrole (GCP) unit to be 5 [31]. Being in excellent agreement with experiments [34]. Therefore, at pH 7.0 only arginine guanidinium and free amino group are protonated, while at pH 5.0 all four protonable fragments are in their ionized cationic forms. Therefore, at pH 7.0, systems **1**–**2** are neutral and **3**–**4** are dicationic, while, at pH 5.0, conjugates **1**–**2** are dicationic and **3**–**4** are tricationic. Accordingly, we submitted all eight systems to molecular dynamics simulations and performed clustering analysis on the obtained structures. Here, we will discuss only the most representative geometries (Fig. 6) that account for the majority of the population of each system, while a complete analysis is placed in the Supporting Information (Fig. S93).

Systems **1** and **2** underwent a larger electrostatic change upon reducing the pH value from 7.0 to 5.0, as these alter their protonation state from neutral to dicationic, while **3** and **4** only increase the overall charge by one, accordingly. Therefore, it was surprising that with **1** not much was changed in the overall population with a change in pH (Fig. 6). Specifically, in the most dominant cluster, around two thirds of all structures (67%) assumed a stretched conformation with no particular intramolecular interactions, and this was consistent under both pH conditions, being in line with its preserved molar absorptivity relative to the reference **Phen-AA**. This clearly leaves the GCP unit available for the interaction with polynucleotides, which was nicely evidenced in roughly the same, yet high affinity of both **1** (at pH 7.0) and $\mathbf{1}^{2+}$ (at pH 5.0) toward ctDNA (Table 2). This notion also helps explaining the pronounced affinity of $\mathbf{1}^{2+}$ toward ss-polynucleotides (Table 4). It also underlines a premise that is evident in other conjugates as well, in which systems that assume stretched conformations are more prone to interactions with biological systems, while those with notable intramolecular interactions that lead to bent or stacked conformations reveal hindered intermolecular recognition [31].

System **2** was an interesting case of a conjugate which exhibited modest interaction with ctDNA at pH 5.0, while being the only molecule which showed no such interactions at all at pH 7.0 (Table 2). At pH 5.0, $\mathbf{2}^{2+}$ undertakes around 47% of structures in the stretched conformation, which was enough to reveal some recognition of ctDNA, yet notably reduced relative to **1** and $\mathbf{1}^{2+}$, being consistent with a reduced percentage of such stretched structures relative to **1** and $\mathbf{1}^{2+}$. This was also in line with decreased interactions of $\mathbf{2}^{2+}$ toward ss-polynucleotides in comparison with $\mathbf{1}^{2+}$ (Table 4). On the other hand, **2** at pH 7.0 showed two distinct clusters, which were both bent and characterized with the π–π stacking interactions involving the GCP pyrrole fragment and the phenanthridine tricycle (Fig. 6) that both account for 92% of structures of **2**. This intramolecular interaction was nicely evident in the evolution of distances between the pyrrole hydrogen and the phenanthridine C1-hydrogen (Fig. S92) that take values mostly between 3 and 8 Å during the entire MD simulation, with the average value of 4.72 Å. This clearly indicates the vicinity of these two hydrogens and confirms a stacked conformation, being fully in line with the reported NOESY spectra (Figs. S6–S9), UV/Vis measurements, and the appearance of bisignate CD signal. The difference among representative clusters in **2** was only in the orientation of the pyrrole fragment that comes as a consequence of the rotation in the C—N single bond between GCP and the glycine moiety. The mentioned stabilisation clearly diminishes the ability of GCP in **2** to interact with other systems as revealed at pH 7.0 here. The difference in the behaviour of **1** and **2** was clearly due to the glycine fragment that connects GCP with phenanthridine. This subtle structural modification introduces a sufficient flexibility in **2** to allow the favourable stacking interactions, which is otherwise too rigid and, therefore, promoting extended conformations as in **1**. As a conclusion, certain rigidity in the overall skeleton of conjugates **1** and **2** is beneficial for their biological activity, which confirms data in Table 2, and serves as a useful guideline in designing even more efficient DNA/RNA probes.

Conjugate **3** also behaved in an already presented manner. Figs. 6 and S93 revealed that a majority of structures in $\mathbf{3}^{2+}$ was stretched, yet 41% of structures were bent, which is a much higher percentage than in $\mathbf{3}^{3+}$, where almost no bent structures were evident. This helps interpreting the slightly reduced interactions of $\mathbf{3}^{2+}$ toward ctDNA relative to $\mathbf{3}^{3+}$.

In general, **3** and **4** with more positive charges are less likely to form bent or stacked geometries than **1** and **2**, due to charge repulsion. In addition, water prefers solvating isolated charges rather than allowing intramolecular interactions. The only notable exception was **4** at pH 7.0, where 53% structures of the dicationic $\mathbf{4}^{2+}$ were found as bent. The latter is facilitated by favourable cation–π interactions between phenanthridine and protonated amino and guanidine moieties (Fig. 6). Still, this system was able to notably bind to ctDNA, being a consequence of 35% of its stretched structures. Yet, the same structural preference was not observed in the analogous $\mathbf{3}^{2+}$ that is more rigid and without a flexible glycine unit, which likely prevents this system from establishing optimal cation–π interactions, thus stretched conformations are preferred. We can assume, given the high charge of $\mathbf{4}^{2+}$, that the transition from the dominant bent to stretched conformations is facile and that it is assisted by the ability of water molecules to solvate charged fragments. On the other hand, $\mathbf{4}^{3+}$ was predominantly found as stretched, thus exhibiting pronounced interactions with ctDNA (Table 2).

In order to check the validity of the premise that **1**–**4** were well represented with the most dominant cluster structures given in Fig. 6, we calculated energies of the excited states responsible for the experimental UV/Vis spectra (Table 1) corresponding to isolated conjugates. For that purpose, we used the most abundant structure of each system in Fig. 6 and performed the geometry optimization by the M06/6–31 G (d) approach with solvent effects modelled through the IEF-PCM explicit water solvation, followed by the TD-DFT computations at the same level of theory. The obtained vertical transitions corresponding to the absorption maxima at pH 7.0 were 292 and 262 nm (**1**), 298 and 268 nm (**2**), 261 nm ($\mathbf{3}^{2+}$), and 271 nm ($\mathbf{4}^{2+}$), while at pH 5.0 were 293 and 260 ($\mathbf{1}^{2+}$), 291 and 261 nm ($\mathbf{2}^{2+}$), 261 nm ($\mathbf{3}^{3+}$), and 261 nm ($\mathbf{4}^{3+}$). These are found in very good agreement with experiments (Table 1), which lends credence to the computational strategy utilized here. This conclusion is further strengthened by the fact that the same approach gave the absorption maximum of 256 nm for the isolated phenanthridine at pH 7.0, which is in excellent agreement with the experimental value of 250 nm, [61] and well matched with 250 nm reported here for **Phen-AA**.

3. Discussion

Summarised results of different methods employed in this work showed that several factors affected the binding of studied compounds to ds- and ss-polynucleotides: 1) differences in the structure and dynamics of studied compounds that relate to the linker length

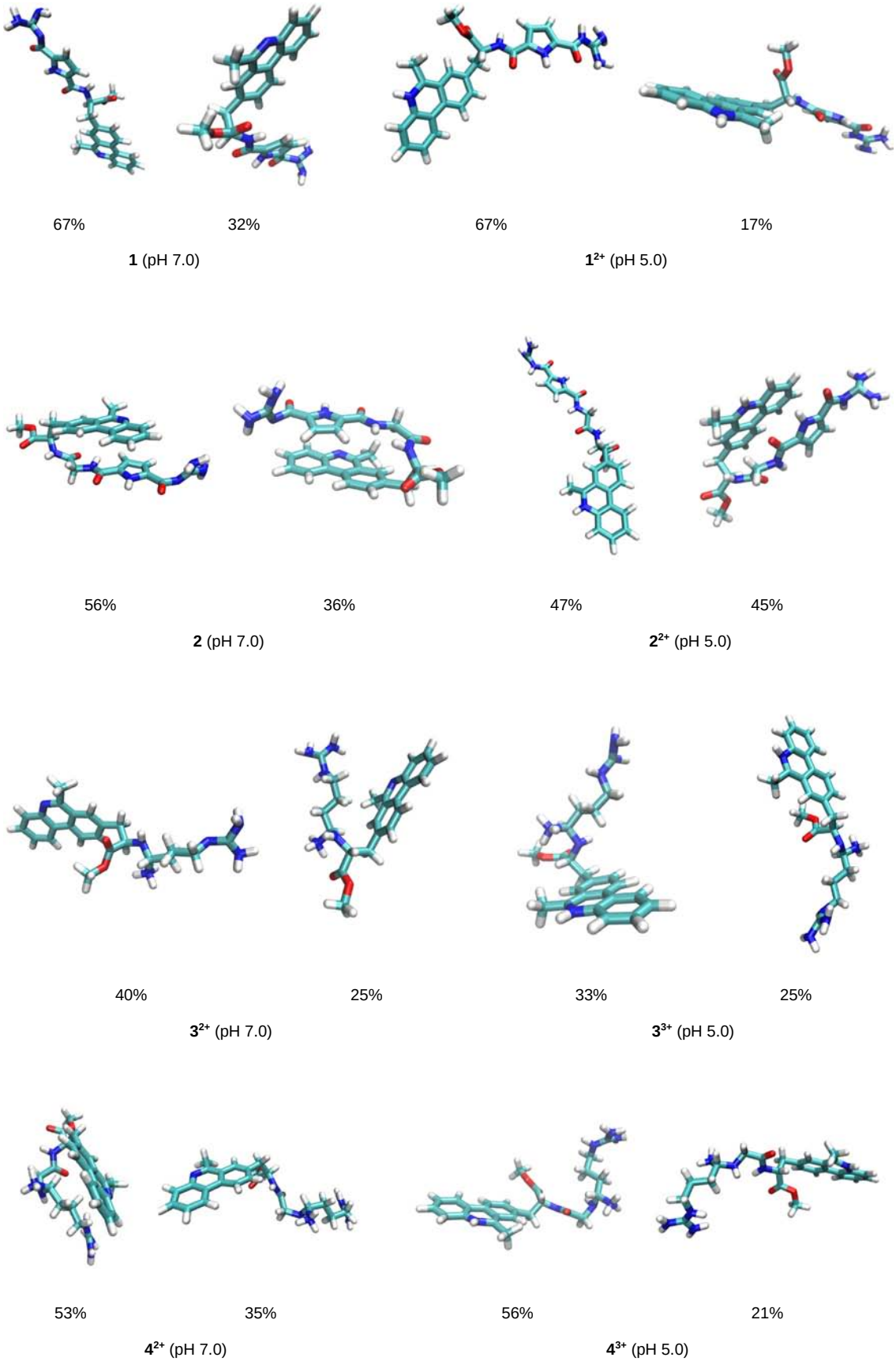

Fig. 6. Most representative structures of conjugates **1**–**4** at different pH conditions and their overall populations during MD simulations. These are identified after the clustering analysis of the corresponding MD trajectories.

(presence/absence of glycine in linker) and the type of the guanidine group (aliphatic guanidine vs pyrrole guanidine) 2) pH of the solution that affects the protonation state of **1**–**4** in neutral and weakly acidic conditions and 3) the secondary structure of the polynucleotides and basepair composition of ds- and ss-polynucleotides.

Smaller number of positive charges of GCP-based peptides in comparison to Arg-based peptides at both pH 7.0 and 5.0 suggests a smaller contribution of the electrostatic interactions in the overall binding of **1**–**2** to polynucleotides. In addition, computations revealed that, in general, conjugates with more positive charge are less likely to form bent or stacked conformations with intramolecular stabilisations prior to binding, which facilitates their interactions with polynucleotides. Further, the guanidine group in the GCP unit has a possibility of additional interaction via pyrrole and acetyl group compared to the arginine guanidinium residue. Furthermore, an elongation of the linker via glycine had different effects on the binding to polynucleotides in GCP- and Arg-based peptides. The stronger binding was obtained for **1** compared to **2** (containing glycine) in GCP series and for **4** (containing glycine) compared to **3** in arginine series. Hypochromic effects and the bisignate signal in CD spectrum of **2** detected at both pH values point to intramolecular aromatic stacking interactions between the phenanthridine and pyrrole units, while noticed shifts of phenanthridine and pyrrole proton signals and cross-peaks between protons of two chromophores also suggested the presence of stacked structure. The linker between chromophores of **2** is long and flexible enough to enable the intramolecular stacking, as confirmed with the computational analysis. The additional proof of the folded conformation of **2** can be found in the study of the interactions with polynucleotides. This is best seen in CD titrations where the CD signals of formed complexes were very similar to intrinsic CD signals of **2** indicating that **2** binds to polynucleotides in the folded conformation. Summarised results of the interaction study (weak binding at pH 7.0 and stronger binding at pH 5.0, small temperature stabilisation of ctDNA at pH 5.0, CD signals of complexes resembling the intrinsic CD signals of **2**), suggest an aggregation as a dominant binding mode of **2** with all polynucleotides. Stronger binding of **2** at pH 5.0 could be explained with non-specific electrostatic interactions between positive charges of phenanthridine and GCP unit with DNA/RNA phosphate backbone. On the other hand, summarised analysis of ^{1}H NMR (absence of cross-peaks between two chromophores in NOESY spectrum in D_2O) and CD spectra of **1** (negative CD signals at both pH compared to bisignate CD signal of **2**) as well as shorter linker (absence of glycine) do not support the formation of intramolecularly stacked conformation. Thus, it can be assumed that **1** is predominantly in the extended or open conformation, which is also nicely revealed by MD simulations. Still, in contrast to pH 5.0 where the UV/Vis spectra clearly indicated an absence of intramolecular interaction between phenanthridine and GCP unit, the comparison of the molar absorptivities of **1** and the corresponding references at pH 7.0 point to some influence of intramolecular interactions. This experimental result can be related to the reduced percentage of stretched structures relative to $\mathbf{1}^{2+}$ (Fig. 6, **1** at pH 7.0).

Changes in the CD spectra at pH 7.0 (negative ICD signals similar but of lower intensity than the intrinsic CD signals of **1**) as well as the absence of stabilisation effects of ds-DNA and RNA suggest the aggregation of **1** along the polynucleotide backbone, probably inside the hydrophobic major grooves.

Significant stabilisation effects of AT-DNA and ctDNA and positive ICD signals in CD titrations with ctDNA, AT- and GC-DNA point to minor groove binding at pH 5.0. [62] Binding of **1** to poly A-poly U resulted also in positive ICD signal near 312 nm. Nevertheless, the absence of ds-RNA stabilisation as well as dimensions of minor groove (broad and very shallow [55]) point to major groove as the dominant binding site.

Peptide **1** could differentiate between dGdC, dAdT and rArU sequences by the differently positioned ICD signal maximums. More important it was able to distinguish between different small molecule binding sites of ds-DNA and ds-RNA by intensity of ICD signals at 295 nm which for DNA- (AT and GC) induced CD bands was strong and for RNA-(AU) ICD band zero. In spite of the same number of charges of arginine derivatives, peptide **4** showed the stronger binding than peptide **3**, which emphasized the significance of the linker length. Obviously, the longer and flexible linker of **4** enabled the better positioning of the guanidine group toward the polynucleotide binding sites than the shorter linker of **3**. Results from the binding study with compound **4** (high binding affinities at both pH, stronger stabilisation effects of DNA and RNA at pH 5.0, weak negative ICD signals) suggest an intercalation as a dominant binding mode in neutral conditions. In weakly acidic conditions, the intercalative binding is accompanied by electrostatic interactions of the positively charged **4** (three positive charges) and the negatively charged polynucleotide phosphates.

The binding affinities in titrations with all studied ss-polynucleotides were dependent on the structure of a compound added. Among studied compounds, GCP-derivative **1** exhibited the highest binding affinities toward ss-polynucleotides (Table 4), especially toward poly rG, rU and dT [63–65]. Its analogue **2** bound only to poly A, poly G and poly C with moderate binding affinities which, as in case of ds-polynucleotides, emphasized the significance of a linker length and flexibility on DNA/RNA binding. The negative ICD signals around 300 nm supported the intercalation of **1** into ss-polynucleotides at lower ratios, *r* while the appearance of positive ICD signals at higher ratios, *r* with most of studied polynucleotides except with poly C and poly dA, point to additional interactions of **1** GCP unit with ss-structures. Changes of CD signals with ss-polynucleotides (Supplementary, Figs. S78, S80 and S82) similar to those in titrations with ds-polynucleotides point to binding of **2** in the form of aggregates along the polynucleotide backbone. Among Arg-based peptides, compound **4**, with longer linker, revealed stronger affinity toward polypurine sequences especially toward poly G. In addition, **4** showed weak negative ICD signals at $\lambda > 300$ nm only with poly A and poly G which points to the intercalation as a dominant binding mode. Compounds **1** and **4** revealed significantly higher affinity toward ds- and ss-polynucleotides in comparison to **2** and **3** which clearly points to significant contribution of structural factors (GCP unit and shorter linker for **1** and longer linker and arginine guanidinium group for **4**) on DNA and RNA binding. Further, stronger interactions of **1** compared to **4** and especially **3**, toward ss-polynucleotides point to the significance of GCP unit that enables additional interactions (hydrogen bonds, hydrophobic interactions and electrostatic interactions) with DNA and RNA sequences. The impact of GCP unit is also seen in an efficient ss-polynucleotide organization induced by **1** (Fig. 5).

All tested compounds exhibited very modest toxicity in vitro which is a desirable feature for potential spectrophotometric probes (Supplementary, Fig. S95).

4. Conclusion

In conclusion, the obtained data demonstrated how minor changes in the structure of short fluorescent peptides **1**–**4** can significantly influence their conformation and the binding to DNA and RNA targets, and in case of **1** and **2** the binding to enzymes (DPP III) [35]. In comparison to binding results of nucleobase–guanidiniocarbonyl-pyrrole conjugates, phenanthridine-guanidine peptides showed better binding affinities to ds- but also ss-polynucleotides [31]. Thus, the fine tuning of structural features of **1** and **4** in future research offers a promising route toward more selective interactions toward DNA/RNA, particularly toward ss-polynucleotides due to a small number of ligands that are highly selective or specific toward such structures. Such novel structurally upgraded ss- and ds-targeting probes can be used for instance as markers of G-rich DNA sequences important in several biological processes, such as DNA replication, gene expression and recombination [66,67] or in inhibition of double-strand break repairs by binding to RNA-DNA hybrids thus disabling their degradation by RNase H [68]. Especially, the promising CD

discrimination between ds-RNA and ds-DNA as well as ss-polynucleotide recognition (rG, dT, rU) provided by the GCP moiety in **1** could be further tuned by the incorporation of the additional recognition units such as lysine. This modification could also enable the molecule to be positively charged in neutral conditions and thus allow more selective interactions at pH 7.0.

5. Experimental

Synthetic procedures were given in Supplementary.

5.1. Materials and methods

^{1}H NMR and ^{13}C NMR spectra were recorded on a Brucker AV300 or Brucker AV600 (at 300 and 600 MHz) at 25 °C. Chemical shifts (d) were given in parts per million (ppm) relative to tetramethylsilane as an internal standard and coupling constants (*J*) in hertz. The splitting patterns in the ^{1}H NMR spectra are denoted as follows: s (singlet), brs (broad singlet), d (doublet), t (triplet), m (multiplet). Melting points were determined on a Kofler melting points apparatus and are uncorrected. Infrared spectra were recorded on a BOMEM MB 102 spectrophotometer and spectral bands are expressed in 'wave numbers' with the unit cm^{-1}. Mass spectra were obtained using BRUKER micrOTOF spectrometer and Waters Micromass ZQ. The UV/Vis spectra were recorded on a Varian Cary 100 Bio spectrophotometer, CD spectra on JASCO J815 spectrophotometer and fluorescence spectra on a Varian Cary Eclipse spectrophotometer at 25 °C using appropriate 1 cm path quartz cuvettes and microcalorimetric measurements on a MicroCal VP-ITC microcalorimeter. For study of interactions with DNA and RNA, aqueous solutions of compounds buffered to pH 5.0 (sodium cacodylate buffer, $I = 0.05$ moldm^{-3}) and pH 7.0 (sodium cacodylate buffer, $I = 0.05$ moldm^{-3}) were used.

Relative fluorescence quantum yields (Q) were determined by the standard procedure [43]. All samples were purged with argon to displace oxygen, and emission spectra were recorded from 350 to 600 nm and corrected for the effects of time- and wavelength-dependent light-source fluctuations by use of a rhodamine 101 standard, a diffuser and the software provided with the instrument. As the standard we used l-*N*-acetyltryptophanamide (NATA, Fluka, Buchs, Switzerland) with published fluorescence quantum yield Q = 0.14 [44]. The concentration of NATA and **3**–**4** in fluorescence measurements had an optical absorbance below 0.05 at the excitation wavelength while **1**–**2** had optical absorbencies between 0.08 and 0.15 at the excitation wavelength (Experimental conditions in Supplementary).

Polynucleotides were purchased as noted: poly A–poly U, poly $(dGdC)_2$, poly$(dAdT)_2$, calf thymus, ctDNA (Sigma). Polynucleotides were dissolved in Na-cacodylate buffer, $I = 0.05$ mol dm^{-3}, pH 7.0. The calf thymus ctDNA was additionally sonicated and filtered through a 0.45 mm filter [69]. Polynucleotide concentration was determined spectroscopically [70] as the concentration of phosphates. Spectrophotometric titrations were performed at pH 5.0 and pH 7.0 by adding portions of polynucleotide solution into the solution of the studied compound for UV/Vis and fluorimetric experiments and for CD experiments were done by adding portions of compound stock solution into the solution of polynucleotide. In fluorimetric experiments excitation wavelength of $\lambda_{exc} \geq 300$ nm was used to avoid the inner filter effect caused due to increasing absorbance of the polynucleotide. Emission was collected in the range $\lambda_{em} =$ 300–550 nm. For ds-polynucleotides calculations gave values of ratio $n = 0.1$–0.4, but for easier comparison all K_a values were re-calculated for fixed $n = 0.3$. For ss-polynucleotides calculations gave values of ratio $n = 0.1$–0.2, but for easier comparison all K_a values were re-calculated for fixed $n = 0.2$. In most cases values for K_a (Tables 2 and 4) had satisfactory correlation coefficients (>0.99).

Thermal melting curves for DNA, RNA and their complexes with studied compounds were determined as previously described by following the absorption change at 260 nm as a function of temperature [71]. Absorbance of the ligands was subtracted from every curve and the absorbance scale was normalized. T_m values are the midpoints of the transition curves determined from the maximum of the first derivative and checked graphically by the tangent method [70]. The ΔT_m values were calculated subtracting T_m of the free nucleic acid from T_m of the complex. Every ΔT_m value here reported was the average of at least two measurements. The error in ΔT_m is ±0.5 °C.

All ITC titrations were done in 50 mM Na-cacodylate buffer pH 5.0. In ITC titrations ss-RNA (poly G, poly C, poly A and poly U, $c = 3$–9×10^{-3} mol dm^{-3}) were injected from rotating syringe (307 rpm) into the isothermal cell, equilibrated at 25.0 °C, containing 14,406 mL of the compound (**1** and **2**, $c = 0.3$–1×10^{-4} mol dm^{-3}) while the titration of ss-DNA (pdT) with a compound **1** was made differently. Compound **1** ($c = 1.5 \times 10^{-4}$ mol dm^{-3}) was injected from rotating syringe (307 rpm) into the isothermal cell, equilibrated at 25.0 °C, containing 14,406 mL of the ss-DNA (pdT, $c = 5 \times 10^{-5}$ mol dm^{-3}). The spacing between each injection was in the range 300–900 s and initial delay before first injection were in the range 600–2000 s. All solutions used for ITC experiments were degassed prior to use under vacuum (0.64 bar, 10 min) to eliminate air bubbles. Microcalorimetric experiment directly gave three parameters; reaction enthalpy change ($\Delta_r H$), binding constant (K_a) and stoichiometry (n). The value of $\Delta_r G$ was calculated from the binding constant ($\Delta_r G = -RT\ln K$) while the entropy contribution was calculated from the binding enthalpy and Gibbs energy ($T\Delta_r S = \Delta_r H - \Delta_r G$).

5.2. Computational details

In order to sample the conformational flexibility of investigated systems and probe their intrinsic dynamics in the aqueous solution, classical molecular dynamics (MD) simulations were performed employing standard generalized AMBER force fields (ff14SB and GAFF) [72] as implemented within the AMBER16 program package [73]. All structures were subsequently solvated in a truncated octahedral box of TIP3P water molecules spanning a 10 Å thick buffer of solvent molecules around each system, and submitted to periodic simulations where the excess positive charge was neutralized with an equivalent number of chloride anions. Upon gradual heating from 0 K, MD simulations were performed at 300 K for a period of 150 ns, maintaining the temperature constant using the Langevin thermostat with a collision frequency of 1 ps^{-1}. The obtained structures in the corresponding trajectories were clustered based on DBSCAN density-based algorithm [74] according to recommended procedures [75]. The idea behind this computational strategy was to investigate whether intrinsic dynamical features of studied conjugates both affect and can explain their tendency to interact with polynucleotides, which also avoids difficulties and inaccuracies associated with the computational prediction of the structure of single-stranded polynucleotides, as very recently emphasized by Jeddi and Saiz [76]. The mentioned approach recently turned out as very useful in interpreting the affinities of several nucleobase – guanidiniocarbonyl-pyrrole conjugates toward single-stranded RNA systems [31].

To confirm that the described clustering analysis elucidated the most representative structures of each conjugate at both experimental pH values, we proceeded by calculating energies of the excited states responsible for the experimental UV/Vis spectra in Table 1 corresponding to isolated conjugates in the aqueous solution. For that purpose, we used the most abundant structure of each system in Fig. 6 and performed the geometry optimization by the M06/6–31 G(d) model in the Gaussian 09 program package, [77] with the water solvent effects modelled through the IEF-PCM explicit solvation. This was followed by the TD-DFT computations at the same level of theory considering 32 lowest singlet electronic excitations. The choice of this setup was prompted by its recent success in modelling UV/Vis spectra of organic heterocycles in various solvents [78].

List of abbreviations

Ala-Phen	phenanthridine-alanine derivative
Arg	arginine
AT-DNA	double-stranded alternating copolymer, poly$(dAdT)_2$
AU	poly A–poly U
CD	circular dichroism
ctDNA	*calf thymus* DNA
DPP III	dipeptidyl peptidase III
ds-DNA/ds-RNA	double-stranded DNA/double-stranded RNA
$\Delta_r G$	Gibbs free energy
$\Delta_r H$	enthalpy
$\Delta_r S$	entropy
GC-DNA	poly $(dGdC)_2$
GCP	guanidinocarbonyl-pyrrole
ICD	induced CD spectrum
ITC	isothermal titration calorimetry
K_a	equilibrium association constant
n	[bound ligand]/[polynucleotide]
ss-DNA/RNA	single-stranded DNA/single-stranded RNA
T_m	melting temperature

Acknowledgments

This research was funded by Croatian Science Foundation (grants No. IP-2018-01-4694, IP-2018-01-5475 and IP-2014-09-3386).

Author contributions

The manuscript was written through contributions of all authors. All authors have given approval to the final version of the manuscript.

Declaration of competing interest

None.

Appendix A. Supplementary data

Supplementary data to this article can be found online at https://doi.org/10.1016/j.ijbiomac.2019.05.063.

References

[1] Z. Simon, N. Voiculetz, I. Motoc, Specific Interaction and Biological Recognition Processes, CRC Press, Boca Raton, 1993.
[2] H.J. Xi, E. Davis, N. Ranjan, L. Xue, D. Hyde-Volpe, D.P. Arya, Thermodynamics of nucleic acid "shape readout" by an aminosugar, Biochemistry 50 (42) (2011) 9088–9113.
[3] A. Sengar, B. Heddi, A.T. Phan, Formation of G-quadruplexes in poly-G sequences: structure of a propeller-type parallel-stranded G-quadruplex formed by a G(15) stretch, Biochemistry 53 (49) (2014) 7718–7723.
[4] A. Aharoni, N. Baran, H. Manor, Characterization of a multisubunit human protein which selectively binds single stranded d(GA)n and d(GT)n sequence repeats in DNA, Nucleic Acids Res. 21 (22) (1993) 5221–5228.
[5] H. Xi, D. Gray, S. Kumar, D.P. Arya, Molecular recognition of single-stranded RNA: neomycin binding to poly(A), FEBS Lett. 583 (13) (2009) 2269–2275.
[6] J. Sambrook, J. Sambrook, E.F. Fritsch, T. Maniatis, Molecular Cloning: A Laboratory Manual, 2nd ed. ed. Cold Spring Harbor Laboratory Press, New York, 1989.
[7] E. Trinquet, G. Mathis, Fluorescence technologies for the investigation of chemical libraries, Mol. BioSyst. 2 (8) (2006) 381–387.
[8] J. Matic, L.M. Tumir, M.R. Stojkovic, I. Piantanida, Advances in peptide-based DNA/RNA-intercalators, Curr. Protein Pept. Sci. 17 (2) (2016) 127–134.
[9] L.-M. Tumir, M.R. Stojković, I. Piantanida, Come-back of phenanthridine and phenanthridinium derivatives in the 21st century, Beilstein J. Org. Chem. 10 (2014) 2930.
[10] C. Bailly, R.K. Arafa, F.A. Tanious, W. Laine, C. Tardy, A. Lansiaux, P. Colson, D.W. Boykin, W.D. Wilson, Molecular determinants for DNA minor groove recognition: design of a bis-guanidinium derivative of ethidium that is highly selective for AT-rich DNA sequences, Biochemistry 44 (6) (2005) 1941–1952.
[11] N.W. Luedtke, Q. Liu, Y. Tor, Synthesis, photophysical properties, and nucleic acid binding of phenanthridinium derivatives based on ethidium, Biorg. Med. Chem. 11 (23) (2003) 5235–5247.
[12] N.W. Luedtke, Q. Liu, Y. Tor, On the electronic structure of ethidium, Chem Eur J 11 (2) (2005) 495–508.
[13] C. Fraire, P. Lecointe, C. Paoletti, Metabolism of ethidium bromide in rats, Drug Metab. Dispos. 9 (2) (1981) 156–160.
[14] P. Lecointe, N. Bichet, C. Fraire, C. Paoletti, The hepatic metabolism of ethidium bromide to reactive mutagenic species: biochemical and structural requirements, Biochem. Pharmacol. 30 (6) (1981) 601–609.
[15] G. Malojcic, I. Piantanida, M. Marinic, M. Zinic, M. Marjanovic, M. Kralj, K. Pavelic, H.J. Schneider, A novel bis-phenanthridine triamine with pH controlled binding to nucleotides and nucleic acids, Organic & Biomolecular Chemistry 3 (24) (2005) 4373–4381.
[16] D. Saftic, M.R. Stojkovic, B. Zinic, L. Glavas-Obrovac, M. Jukic, I. Piantanida, L.M. Tumir, Impact of linker between triazolyluracil and phenanthridine on recognition of DNA and RNA. Recognition of uracil-containing RNA, New J. Chem. 41 (22) (2017) 13240–13252.
[17] L.-M. Tumir, I. Piantanida, I. Juranović, Z. Meić, S. Tomić, M. Žinić, Recognition of homo-polynucleotides containing adenine by a phenanthridinium bis-uracil conjugate in aqueous media, Chem. Commun. (20) (2005) 2561–2563.
[18] I. Juranović, Z. Meić, I. Piantanida, L.-M. Tumir, M. Žinić, Interactions of phenanthridinium–nucleobase conjugates with polynucleotides in aqueous media. Recognition of poly U, Chem. Commun. (13) (2002) 1432–1433.
[19] L.M. Tumir, I. Piantanida, I.J. Cindrić, T. Hrenar, Z. Meić, M. Žinić, New permanently charged phenanthridinium–nucleobase conjugates. Interactions with nucleotides and polynucleotides and recognition of ds-polyAH , J. Phys. Org. Chem. 16 (12) (2003) 891–899.
[20] M. Dukši, D. Baretić, V. Čaplar, I. Piantanida, Novel bis-phenanthridine derivatives with easily tunable linkers, study of their interactions with DNA and screening of antiproliferative activity, Eur. J. Med. Chem. 45 (6) (2010) 2671–2676.
[21] M. Dukši, D. Baretić, I. Piantanida, Synthesis of the peptide-based phenanthridine-nucleobase conjugates and study of their interactions with ds-DNA, Acta Chim. Slov. 59 (3) (2012).
[22] C.L. Hannon, E.V. Anslyn, The guanidinium group: its biological role and synthetic analogs, Bioorganic Chemistry Frontiers, Springer, Berlin 1993, pp. 193–255.
[23] R.M.C. Dawson, Data for Biochemical Research, Clarendon Press, 1986.
[24] C. Schmuck, M. Heil, J. Scheiber, K. Baumann, Charge interactions do the job: a combined statistical and combinatorial approach to finding artificial receptors for binding tetrapeptides in water, Angew. Chem. Int. Ed. 44 (44) (2005) 7208–7212.
[25] C. Schmuck, M. Heil, Peptide binding by one-armed receptors in water: screening of a combinatorial library for the binding of Val-Val-Ile-Ala, ChemBioChem 4 (11) (2003) 1232–1238.
[26] M. Li, M. Radić Stojković, M. Ehlers, E. Zellermann, I. Piantanida, C. Schmuck, Use of an octapeptide–guanidiniocarbonylpyrrole conjugate for the formation of a supramolecular β-helix that self-assembles into pH-responsive fibers, Angew. Chem. Int. Ed. 55 (42) (2016) 13015–13018.
[27] M. Li, S. Schlesiger, S.K. Knauer, C. Schmuck, A tailor-made specific anion-binding motif in the side chain transforms a tetrapeptide into an efficient vector for gene delivery, Angew Chem Int Edit 54 (10) (2015) 2941–2944.
[28] M. Li, M. Ehlers, S. Schlesiger, E. Zellermann, S.K. Knauer, C. Schmuck, Incorporation of a non-natural arginine analogue into a cyclic peptide leads to formation of positively charged nanofibers capable of gene transfection, Angew Chem Int Edit 55 (2) (2016) 598–601.
[29] M. Li, M. Matkovic, I. Piantanida, C. Schmuck, Incorporation of arginine mimetic residue into peptides for recognition of double stranded nucleic acid structure: binding and aggregation studies, Biorg. Med. Chem. 25 (6) (2017) 1875–1880.
[30] M.R. Stojkovic, P. Piotrowski, C. Schmuck, I. Piantanida, A short, rigid linker between pyrene and guanidiniocarbonyl-pyrrole induced a new set of spectroscopic responses to the ds-DNA secondary structure, Organic & Biomolecular Chemistry 13 (6) (2015) 1629–1633.
[31] Z. Ban, B. Zinic, R. Vianello, C. Schmuck, I. Piantanida, Nucleobase-guanidiniocarbonyl-pyrrole conjugates as novel fluorimetric sensors for single stranded RNA, Molecules 22 (12) (2017) 2213.
[32] F. Huang, W.M. Nau, A conformational flexibility scale for amino acids in peptides, Angew. Chem. Int. Ed. 42 (20) (2003) 2269–2272.
[33] J. Jacob, H. Duclohier, D.S. Cafiso, The role of proline and glycine in determining the backbone flexibility of a channel-forming peptide, Biophys. J. 76 (3) (1999) 1367–1376.
[34] C. Schmuck, H.Y. Kuchelmeister, Guanidinium based anion receptors, Artificial Receptors for Chemical Sensors, Wiley-VCH Verlag GmbH & Co. KGaA, Weinheim, Germany, 2010.
[35] J. Matić, F. Šupljika, N. Tir, P. Piotrowski, C. Schmuck, M. Abramić, I. Piantanida, S. Tomić, Guanidiniocarbonyl-pyrrole-aryl conjugates as inhibitors of human dipeptidyl peptidase III: combined experimental and computational study, RSC Adv. 6 (86) (2016) 83044–83052.
[36] L.M. Tumir, I. Piantanida, P. Novak, M. Zinic, Interactions of novel phenanthridinium-nucleobase conjugates with complementary and non-complementary nucleotides in aqueous media, J. Phys. Org. Chem. 15 (8) (2002) 599–607.
[37] J.W. Lown, B.C. Gunn, K.C. Majumdar, E. Mcgoran, Synthesis of potential DNA bis-intercalative agents of the phenanthridinium class, Canadian Journal of Chemistry-Revue Canadienne De Chimie 57 (17) (1979) 2305–2313.
[38] J. Xi, Q.L. Dong, G.S. Liu, S.Z. Wang, L. Chen, Z.J. Yao, Efficient synthesis of phenanthridines using Hendrickson reagent initiated cascade reaction under mild conditions, Synlett (11) (2010) 1674–1678.

[39] B.M. Trost, M.T. Rudd, Chemoselectivity of the ruthenium-catalyzed hydrative diyne cyclization: total synthesis of ()- cylindricine C, D, and E, Org. Lett. 5 (24) (2003) 4599–4602.
[40] S. Tabanella, I. Valancogne, R. F.W. Jackson, Preparation of enantiomerically pure pyridyl amino acids from serine, Organic & Biomolecular Chemistry 1 (23) (2003) 4254–4261.
[41] C. Schmuck, Side chain selective binding of N-acetyl-α-amino acid carboxylates by a 2-(guanidiniocarbonyl) pyrrole receptor in aqueous solvents, Chem. Commun. (9) (1999) 843–844.
[42] C. Schmuck, Carboxylate binding by 2-(guanidiniocarbonyl) pyrrole receptors in aqueous solvents: improving the binding properties of guanidinium cations through additional hydrogen bonds, Chem Eur J 6 (4) (2000) 709–718.
[43] J. Miller, Standards for Fluorescence Spectrometry, Chapman and Hall, London, 1981.
[44] M.R. Eftink, J. Jia, D. Hu, C.A. Ghiron, Fluorescence studies with tryptophan analogs: excited state interactions involving the side chain amino group, J. Phys. Chem. 99 (15) (1995) 5713–5723.
[45] D. Gargiulo, F. Derguini, N. Berova, K. Nakanishi, N. Harada, Unique ultraviolet-visible and circular-dichroism behavior due to exciton coupling in a biscyanine dye, J. Am. Chem. Soc. 113 (18) (1991) 7046–7047.
[46] N. Berova, L. Di Bari, G. Pescitelli, Application of electronic circular dichroism in configurational and conformational analysis of organic compounds, Chem. Soc. Rev. 36 (6) (2007) 914–931.
[47] N. Berova, Koji Nakanishi's enchanting journey in the world of chirality, Chirality 9 (5–6) (1997) 395–406.
[48] J. Parish, Principles of nucleic acid structure: by W Saenger. pp 556. Springer-Verlag, New York. 1984. DM 79. ISBN 3-540-90761-0, Biochem. Mol. Biol. Educ. 13 (2) (1985) 92.
[49] S.A.E. Marras, F.R. Kramer, S. Tyagi, Efficiencies of fluorescence resonance energy transfer and contact-mediated quenching in oligonucleotide probes, Nucleic Acids Res. 30 (21) (2002).
[50] S.O. Kelley, J.K. Barton, Electron transfer between bases in double helical DNA, Science 283 (5400) (1999) 375–381.
[51] M.R. Stojkovic, S. Miljanic, K. Miskovic, L. Glavas-Obrovac, I. Piantanida, The phenanthridine biguanides efficiently differentiate between dGdC, dAdT and rArU sequences by two independent, sensitive spectroscopic methods, Mol. BioSyst. 7 (5) (2011) 1753–1765.
[52] G. Scatchard, The attractions of proteins for small molecules and ions, Ann. N. Y. Acad. Sci. 51 (1) (1949) 660–672.
[53] B.S. Palm, I. Piantanida, M. Žinić, H.-J. Schneider, The interaction of new 4, 9-diazapyrenium compounds with double stranded nucleic acids, J. Chem. Soc. Perkin Trans. 2 (2) (2000) 385–392.
[54] G.M. Blackburn, M. Gait, D. Loakes, David M. Williams, Nucleic Acids in Chemistry and Biology, Royal Society of Chemistry, Cambridge, 2006.
[55] C. Cantor, P. Schimmel, I.I.I. Part, The Behavior of Biological Macromolecules, Biophysical Chemistry, WH Freeman and Company, New York, 1980.
[56] M. Eriksson, B. Nordén, Linear and circular dichroism of drug-nucleic acid complexes, Methods Enzymol. 340 (2001) 68–98.
[57] A. Rodger, B. Nordén, Circular Dichroism and Linear Dichroism, Oxford University Press, 1997.
[58] N. Berova, K. Nakanishi, R.W. Woody, Circular Dichroism: Principles and Applications, 2nd ed. Wiley-VCH, New York, 2000.
[59] B. Cox, Acids and Bases: Solvent Effects on Acid-Base Strength, Oxford University Press, 2013.
[60] R. Borštnar, M. Repič, S. Kamerlin, R. Vianello, J. Mavri, Computational study of the pKa values of potential catalytic residues in the active site of monoamine oxidase B, J. Chem. Theory Comput. 8 (2012) 3864–3870.
[61] K. Wiesner, S. Figdor, M. Bartlett, D. Henderson, Garrya alkaloids: I. the structure of garryine and veatchine, Can. J. Chem. 30 (1952) 608–626.
[62] A.Y. Chen, C. Yu, B. Gatto, L.F. LIu, DNA minor groove-binding ligands: a different class of mammalian DNA topoisomerase I inhibitors, Proc. Natl. Acad. Sci. 90 (17) (1993) 8131–8135.
[63] S. Wang, E.T. Kool, Origins of the large differences in stability of DNA and RNA helixes: C-5 methyl and 2′-hydroxyl effects, Biochemistry 34 (12) (1995) 4125–4132.
[64] M.R. Stojković, M. Škugor, S. Tomić, M. Grabar, V. Smrečki, Ł. Dudek, J. Grolik, J. Eilmes, I. Piantanida, Dibenzotetraaza [14] annulene–adenine conjugate recognizes complementary poly dT among ss-DNA/ss-RNA sequences, Organic & biomolecular chemistry 11 (24) (2013) 4077–4085.
[65] L. Racane, R. Stojkovic, V. Tralic-Kulenovic, H. Ceric, M. Dakovic, K. Ester, A.M. Krpan, M.R. Stojkovic, Interactions with polynucleotides and antitumor activity of amidino and imidazolinyl substituted 2-phenylbenzothiazole mesylates, Eur. J. Med. Chem. 86 (2014) 406–419.
[66] G. Saretzki, Telomerase inhibition as cancer therapy, Cancer Lett. 194 (2) (2003) 209–219.
[67] L.B. Yuan, T. Tian, Y. Chen, S.Y. Yan, X.W. Xing, Z.A. Zhang, Q.Q. Zhai, L. Xu, S.O. Wang, X.C. Weng, B.F. Yuan, Y.Q. Feng, X. Zhou, Existence of G-quadruplex structures in promoter region of oncogenes confirmed by G-quadruplex DNA cross-linking strategy, Sci Rep-Uk 3 (2013).
[68] C. Ohle, R. Tesorero, G. Schermann, N. Dobrev, I. Sinning, T. Fischer, Transient RNA-DNA hybrids are required for efficient double-strand break repair, Cell 167 (4) (2016) 1001–1013.
[69] J.B. Chaires, N. Dattagupta, D.M. Crothers, Studies on interaction of anthracycline antibiotics and deoxyribonucleic acid: equilibrium binding studies on the interaction of daunomycin with deoxyribonucleic acid, Biochemistry 21 (17) (1982) 3933–3940.
[70] E. Chargaff, R. Lipshitz, Composition of mammalian desoxyribonucleic acids1, J. Am. Chem. Soc. 75 (15) (1953) 3658–3661.
[71] J.-L. Mergny, L. Lacroix, Analysis of thermal melting curves, Oligonucleotides 13 (6) (2003) 515–537.
[72] J.M. Wang, R.M. Wolf, J.W. Caldwell, P.A. Kollman, D.A. Case, Development and testing of a general amber force field, J. Comput. Chem. 25 (9) (2004) 1157–1174.
[73] D. Case, R. Betz, D.S. Cerutti, T. Cheatham, T. Darden, R. Duke, T.J. Giese, H. Gohlke, A. Götz, N. Homeyer, S. Izadi, P. Janowski, J. Kaus, A. Kovalenko, T.-S. Lee, S. LeGrand, P. Li, C. Lin, T. Luchko, P.A. Kollman, Amber 2016, University of California, San Francisco, 2016.
[74] M. Ester, H. Kriegel, J. Sander, X. Xu, A density-based algorithm for discovering clusters a density-based algorithm for discovering clusters in large spatial databases with noise, KDD '96 Proceedings of the Second International Conference on Knowledge Discovery and Data Mining, AAAI Press ©1996, Portland, Oregon 1996, pp. 226–231.
[75] J.Y. Shao, S.W. Tanner, N. Thompson, T.E. Cheatham, Clustering molecular dynamics trajectories: 1. Characterizing the performance of different clustering algorithms, J. Chem. Theory Comput. 3 (6) (2007) 2312–2334.
[76] I. Jeddi, L. Saiz, Three-dimensional modeling of single stranded DNA hairpins for aptamer-based biosensors, Sci Rep-Uk 7 (2017) 1178.
[77] M.J. Frisch, G.W. Trucks, H.B. Schlegel, G.E. Scuseria, M.A. Robb, J.R. Cheeseman, G. Scalmani, V. Barone, G.A. Petersson, H. Nakatsuji, X. Li, M. Caricato, A.V. Marenich, J. Bloino, B.G. Janesko, R. Gomperts, B. Mennucci, H.P. Hratchian, J.V. Ortiz, A.F. Izmaylov, J.L. Sonnenberg, F. Ding Williams, F. Lipparini, F. Egidi, J. Goings, B. Peng, A. Petrone, T. Henderson, D. Ranasinghe, V.G. Zakrzewski, J. Gao, N. Rega, G. Zheng, W. Liang, M. Hada, M. Ehara, K. Toyota, R. Fukuda, J. Hasegawa, M. Ishida, T. Nakajima, Y. Honda, O. Kitao, H. Nakai, T. Vreven, K. Throssell, J.A. Montgomery Jr., J.E. Peralta, F. Ogliaro, M.J. Bearpark, J.J. Heyd, E.N. Brothers, K.N. Kudin, V.N. Staroverov, T.A. Keith, R. Kobayashi, J. Normand, K. Raghavachari, A.P. Rendell, J.C. Burant, S.S. Iyengar, J. Tomasi, M. Cossi, J.M. Millam, M. Klene, C. Adamo, R. Cammi, J.W. Ochterski, R.L. Martin, K. Morokuma, O. Farkas, J.B. Foresman, D.J. Fox, Gaussian 16 Rev. B.01, Wallingford, CT 2016.
[78] M. Hranjec, E. Horak, D. Babic, S. Plavljanin, Z. Srdovic, I.M. Steinberg, R. Vianello, N. Perin, Fluorescent benzimidazo[1,2-a]quinolines: synthesis, spectroscopic and computational studies of protonation equilibria and metal ion sensitivity, New J. Chem. 41 (1) (2017) 358–371.